Observation of self-amplified spontaneous emission in the near-infrared and visible wavelengths

M. Babzien,[1] I. Ben-Zvi,[1] P. Catravas,[2] J.-M. Fang,[3] T. C. Marshall,[3] X. J. Wang,[1] J. S. Wurtele,[4] V. Yakimenko,[1] and L. H. Yu[1]

[1]*National Synchrotron Light Source, Brookhaven National Laboratory, Upton, New York 11973*

[2]*Massachusetts Institute of Technology, Cambridge, Massachusetts 02139*

[3]*Department of Applied Physics, Columbia University, New York, New York 10027*

[4]*Department of Physics, University of California at Berkeley, Berkeley, California 94720*

(Received 7 November 1997; revised manuscript received 12 January 1998)

We report evidence of self-amplified spontaneous emission (SASE) at 1064 and 633 nm. To our knowledge, these are the first measurements of SASE at such a short wavelength and employ the smallest period wiggler, 8.8 mm, used to date in a successful SASE experiment. The experiments were performed with the MIT microwiggler at the Accelerator Test Facility at BNL. Single-pass, on-axis microwiggler emissions within a 25 nm bandwidth have been recorded as a function of beam charge and show a clear enhancement over spontaneous emission. For the measurement at 1064 nm, a single micropulse at 34 MeV with a variable charge of 0–1 nC and less than 5 ps full width at half maximum bunch length was passed through the microwiggler and emissions into a limited solid angle and bandwidth, selected by an aperture and interference filter, were focused onto a silicon photodiode. Enhancement of the emissions, from 2 to 6 times the spontaneous emission level, was observed at the highest charges. In addition, we observed SASE gain at a wavelength of 633 nm at a beam energy of 48 MeV, without detailed measurements. [S1063-651X(98)06805-6]

PACS number(s): 41.60.Cr

I. INTRODUCTION

Understanding the physics of self-amplified spontaneous emission (SASE) in a free-electron laser (FEL) has been a subject of considerable theoretical and experimental effort in recent years. This research has been motivated by the possibility of using a FEL operating in the SASE mode to produce high-brightness x rays. In the SASE mode of operation, a high-current electron beam propagates through a long wiggler and amplifies its own spontaneous emission. The physics of a SASE FEL is not sufficiently characterized and has only been demonstrated at wavelengths separated by up to four orders of magnitude from proposed devices [1,2].

Initial experiments were conducted at microwave frequencies and more recent experiments have been reported at 12–5 μm [2–8]. Moving studies toward shorter wavelengths is technically challenging because of tighter demands on the quality of the system. Longer-wavelength experiments are favored by higher gain and less sensitivity to emittance and energy spread. Experiments at longer wavelength have noted that the amplified noise is greater than would be expected from shot-noise theory. In the microwave region this is not surprising since the frequency separation between microwaves, the beam pipe cutoff (characteristic of wake fields), and beam plasma frequency is not great. In far infrared wavelength experiments the large ratio of wavelength to bunch length can provide coherent enhancement of spontaneous emission without SASE gain. Levels of coherent enhancement of four orders of magnitude have been reported by several groups [9,10] working in the far-infrared region. These experiments, therefore, cannot study the growth of coherent radiation from spontaneous emission or particle noise, which is the operative mechanism expected for forthcoming x-ray FEL experiments.

We report a demonstration of the startup of SASE at 1 μm and preliminary results at 633 nm, which, to our knowledge, is the first observation of its kind at visible wavelengths. We have performed a check, using transition radiation, for coherent spontaneous emission and find none. Furthermore, while previous work generally made use of long-period wigglers, having periods on the order of 5 cm, we have used a microwiggler in these experiments. Our experimental results are consistent with theoretical and numerical predictions.

This paper is organized as follows. In Sec. II we describe the experimental set-up, in Sec. III we present the measurements, in Sec. IV we briefly describe the theory and compare with experiments, and in Sec. V we present conclusions.

II. EXPERIMENTAL SETUP

The electron beam at the Brookhaven Accelerator Test Facility (ATF) [11] is produced by a high-brightness photocathode rf gun [12] and accelerated up to 60 MeV by two *S*-band linear accelerator sections. The drive laser illuminating the magnesium cathode has a pulse duration of 10 ps full width at half maximum (FWHM). The transport line consists of three 20° dipole magnets and multiple quadrupole magnets. The dispersive section between the first two dipoles enables measurement of the beam energy spread and, using a collimating slit, control of the beam charge. The nominal beam parameters are energy spread 0.15% rms and 2×10^{-6} m rad rms normalized emittance. Our definition of the rms emittance is given in Sec. III A. The exact values depend on other beam parameters and will be given below. Diagnostics include phosphor-coated flags, stripline beam position monitors, and Faraday cups. More information on the ATF can be found in Ref. [11].

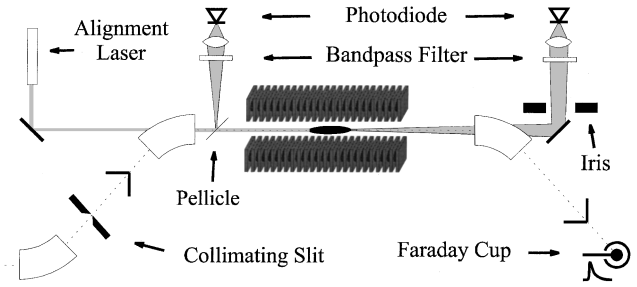

FIG. 1. Experimental configuration showing the salient diagnostics for the optical radiation and the electron beam measurements. Moving from left to right, the collimating slit after the first bending magnet is used to select a longitudinal slice; the pellicle after the second bending magnet and the photodiode are used for the optical transition radiation measurements; the mirror, iris, filter, lens, and photodiode are used for the optical emission measurement; and the Faraday cup is used for beam charge measurements.

The MIT microwiggler is a tunable, pulsed electromagnet with a period of 8.8 mm, which provides a peak on-axis field of 0.45 T. Sixty-one periods were used for these experiments. Each of the half periods is individually adjustable and a tuning procedure is employed that consistently provides rms spreads in the peak field of better than 0.1%, thus providing the field quality essential for research in short-wavelength generation. Further details of the MIT microwiggler construction and capabilities have been published elsewhere [13,14].

A schematic of the experiment components is shown in Fig. 1. Located on either end of the wiggler are two multifunction diagnostic ports. Designed to provide a means for precision coalignment of the wiggler axis and electron beam trajectory, these ports employ three-position pneumatic translators. One position places a phosphor screen on axis where it can be imaged by a charge coupled device (CCD) camera to visualize the electron beam or helium neon alignment laser distribution. A second position inserts a 45° pellicle beam splitter. In addition to coupling out on-axis light from the alignment laser or wiggler, the pellicle acts as a transition radiation screen. The pellicle is imaged onto a CCD camera or the light may be focused onto a silicon photodiode.

The wiggler emission is normally collected after the third dipole separates the photons and electrons. The emission is passed through a variable diameter iris diaphragm to limit collection angle and an interference filter to limit bandwidth. A focusing lens concentrates all optical emission onto a silicon avalanche photodiode that has enhanced infrared quantum efficiency. The diode signal is measured through an amplifier with a digitizing oscilloscope. The responsivity of this optoelectronic system was calibrated with the photocathode drive laser at 1064 nm and agrees well with expectations based on specifications of the individual components.

The ATF provides optical pulses from the photocathode drive laser that mimic the wiggler emission very closely in both wavelength and temporal structure, allowing good calibration and preparation to be performed. The entire optical system is very robust.

III. EXPERIMENTAL RESULTS

A. Electron beam measurements

In order to provide data that can be inserted into theoretical models, the electron beam must be characterized. Important beam parameters measured are the longitudinal current distribution, emittance, and energy spread. These measurements are needed to check that the wiggler emissions are consistent with theoretical and numerical predictions.

The current distribution is measured by changing the rf phase of the second linear accelerator section to produce a linear dependence of the particle energy (relative to a nominal energy) on longitudinal position or arrival time at the slit [15]. The collimating slit in the dispersive region acts as a filter, which passes only a narrow slice in time. The precision of this method is limited by the stability of the rf system, which is approximately ± 1 ps, and the intrinsic energy spread of the bunch, which at $<0.3\%$ corresponds to 0.7 ps. A Faraday cup and charge-sensitive analog-to-digital converter are used to measure transmitted charge and the rf phase of the second linear accelerator section is scanned. The absolute phase and relative phase shift are used to calibrate the time scale.

The result of the SASE calculation depends sensitively on the beam density in six-dimensional phase space. In particular, the transverse emittances are used, in simulation and theory, to parametrize the beam distribution in the two transverse phase spaces (p_x,x) and (p_y,y). We measured the emittance using two methods: the quadrupole magnet scan and a two-screen method. Since we cannot make a complete mapping of the beam distribution in phase space, we follow a common practice and approximate the distribution by an ellipse in each transverse phase space. The measured parameters (ellipse area, aspect ratio, and orientation) are represented by the symmetric beam matrix

$$\Sigma = \begin{pmatrix} \sigma_{11} & \sigma_{12} \\ \sigma_{21} & \sigma_{22} \end{pmatrix},$$

where $\sigma_{12}=\sigma_{21}$ is the correlation, $\sqrt{\sigma_{11}}$ is the beam size, and $\sqrt{\sigma_{22}}$ is the beam divergence. The beam line is designed so that coupling among different dimensions is negligible in the operating regime. We define the geometrical emittance as $\varepsilon = \sqrt{\sigma_{11}\sigma_{22}-\sigma_{12}^2}$. The normalized emittance is then given by $\varepsilon_n=\gamma\varepsilon$. For the emittance measurement using the quadrupole magnet scan technique the measured beam size $\sqrt{\sigma_{11}^m}$ is related to the beam matrix at the entrance of the varying quadrupole magnet by

$$\sigma_{11}^m = R_{11}^2\sigma_{11} + 2R_{11}R_{12}\sigma_{12} + R_{12}^2\sigma_{22},$$

where R_{ij} are the elements of the beam transfer matrix for the measurement region (from the quadrupole magnet entrance to the beam profile monitor). When the measured beam size is obtained by taking the second moment of the intensity vs position distribution, the resulting beam matrix and derived emittance are designated as rms quantities. The beam matrix at the entrance of the quadrupole magnet represents three parameters that are the variables in a best-fit

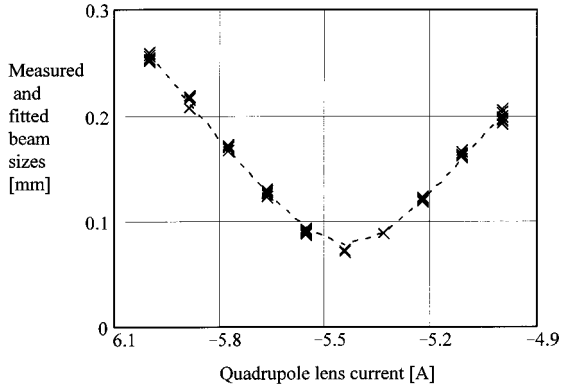

FIG. 2. Beam size vs quadrupole current for a quadrupole scan emittance measurement. The measured points are marked by ×'s and the dashed line is the fit by which we determine the emittance.

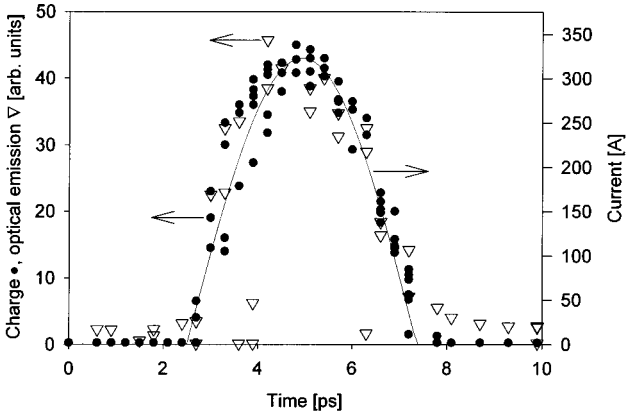

FIG. 3. Longitudinal slice charge (●), wiggler emission (▽), and current (solid line) as a function of time along the electron bunch. This is a ''slice'' measurement, providing a determination of the local peak current and the optical emissions as a function of time along the bunch. The resolution is better than 1 ps. The peak current at the center of the bunch is 320 A.

procedure. Typical quadrupole scan data, corresponding to the normalized rms emittance $\varepsilon_N = 3.2$ mm mrad for a 0.8-nC charge, are shown in Fig. 2.

That method gives information about the second moment only. The greatest uncertainty is related to the calculation of the measured beam size from the camera image. We used, for those measurements, a camera with a dynamic range of 8 bits. The natural noise of the camera (with closed iris) was measured to be about 23 (in the range of 0–255). The value 23 was subtracted as a background before the second moment was calculated. As the beam size changed during the scan, the image intensity also varied and with it the sensitivity to the background, thus introducing a measurement error.

A second method was also used to characterize the second moment of the beam distribution: the two-screen method. The distance between the two monitors (located at a beam line nearly identical to the wiggler beam line) was 4 m. The last quadrupole magnet was used to minimize the beam size at the second screen. The emittance is related to the measured beam sizes by

$$\varepsilon_N = \frac{\sigma_1 \sigma_2}{L}\,\gamma,$$

where σ_1 and σ_2 are measured beam sizes at the first and second beam profile monitors, correspondingly, L is the distance between the two screens, and γ is the average beam energy in units of the electron's rest mass. The results of the two-screen beam measurements are presented in Table I for two cases: the full beam and a beam slice.

Because the beam intensity variation did not affect our measurements (irises on both monitors were adjusted to use the whole dynamic range of the cameras), we may conclude that the two-screen method is less sensitive to the limited dynamic range of the camera. However, it is important to remember that both emittance measurement methods involve *a priori* assumptions on the beam distribution in phase space. Furthermore, these two techniques may be measuring dissimilar attributes of the electron beam distribution. Since we do not have access to the actual beam distribution in phase space, this is the best characterization that can be done. A single number (the emittance) cannot represent faithfully an unknown distribution function and one need not expect complete agreement with measurement by another technique. Likewise, a theoretical prediction for a result (such as FEL gain) or a simulation, which require assumptions on the beam distribution in phase space, need not agree with the measured result, i.e., gain, even though the measured emittance is used as input into the theory.

TABLE I. Emittance measurement for the complete beam and for a longitudinal slice.

	Charge (pC)	Beam sizes (mm)		Normalized emittance (mm rad)
		σ_1	σ_2	
full beam	900	1.02	0.12	2.4
beam slice	80	0.73	0.09	1.2

In the SASE measurements, the charge of the beam is varied using the collimating slit after the first dipole. The beam tune after the linac can be set so that the beam size at the slit is dominated by betatron distribution, not by the very-low-energy spread produced at the ATF. This is verified using additional screens after the collimating slit. A discussion of the effect of changes in the beam parameters (due to the changes in the slit width) on the optical measurements is presented in Sec. III B.

A measurement of the beam peak current vs the longitudinal position (or time) was taken after SASE was observed and is shown in Fig. 3. This measurement serves two purposes. First, it provides us with a measurement of the electron bunch length and longitudinal distribution. In addition, by measuring the optical emission from the wiggler along the bunch, we can verify that the optical emission intensity is just proportional to the local peak current. This serves to remove a possible mechanism that might mimic SASE in the slit scan technique.

The full beam charge delivered to the Faraday cup for this measurement is 0.8 nC. The short pulse duration, almost $\frac{1}{3}$ the drive laser duration, and corresponding high beam current is caused in part by rf compression in the gun. The very

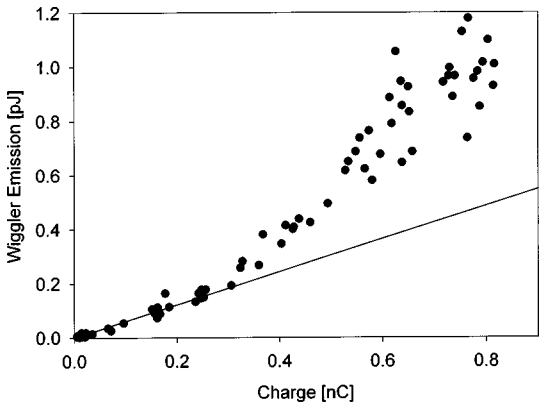

FIG. 4. Charge dependence of wiggler emission at 1064 nm. The solid line is a fit to the spontaneous emission at low charge (optical emission before SASE sets in). Each point is an independent measurement pair of optical energy and beam charge. The scatter of the points results from the startup mechanism of SASE (see the text).

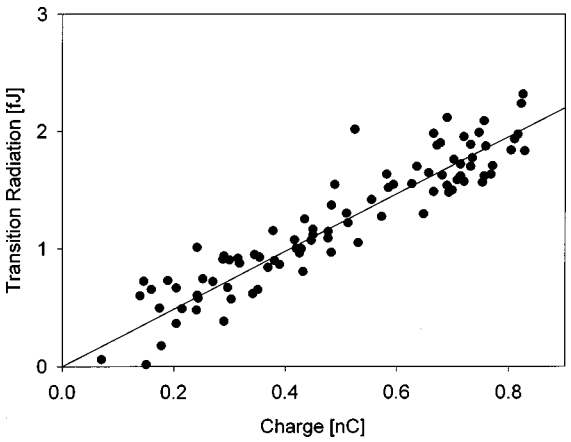

FIG. 5. Charge dependence of transition radiation at 1064 nm. The transition radiation is linear with charge. This is evidence against coherent emission due to micro-bunching and for SASE as the mechanism for the enhancement of optical emission from the wiggler at high charge at the wavelength of interest.

high quantum efficiency of the magnesium photocathode used is also important, although the measured distribution is not well explained by present theory of pulse evolution in a rf gun. Several parameters contributing to the high peak current are not easily measured directly or controlled; therefore, day to day variations in current were observed. This made it necessary to measure the longitudinal pulse distribution at least once during every run.

B. Optical measurements

The charge dependence of emissions from the wiggler in a 25 nm bandwidth around 1064 nm and an opening of 1.0×10^{-3} rad (half-angle) about the central axis of the wiggler is shown in Fig. 4. The straight line represents the expected spontaneous emission dependence, as extrapolated from the low charge points, if variation of the beam distribution, such as energy spread and emittance, are not included. A detailed discussion of such dependence will be presented elsewhere [16].

When the beam pulse charge is varied, one may expect some variation of beam parameters (such as emittance) that affect the radiation spectrum or directionality. This raises the possibility that the resulting alteration of line shape could cause radiation at wavelengths or directions that fall outside of the bandwidth of the optical filter or the acceptance of the optical system. The FWHM of the spontaneous wiggler radiation emitted along the axis of the FEL is $1/N_w = 1.6\%$. The filter linewidth accepts radiation having a somewhat larger range of wavelengths (2.4%). Taking the emittance observed ($\varepsilon_N = 2.4$ mm mrad) at the maximum charge and a beam radius of 0.3 mm, we find the expected emittance inhomogeneous broadening of the spontaneous line falls well within the $1/N_w$ bandwidth; this is true for the energy spread ($\Delta E/E = 0.3\% < 1/4N_w = 0.4\%$) and variation as well. The same conclusions apply to radiation that falls within the cone of light that can be detected by the optical system since the half-width angle of the radiation cone that can be accepted corresponds to a bandwidth that is nearly the same as the actual filter bandwidth. Thus the expected contributions of the inhomogeneous effects on the radiation linewidth and angular divergence are less than the $1/N_w$ bandwidth that the optical system is designed to accept, for the full range of bunch charge variation. If the beam charge is reduced, then the inhomogeneous effects become even less. Line-narrowing effects with increasing SASE gain will be accepted by the optical system. Our conclusion is that as the bunch charge is varied, the optical system records the correct mixture of axially directed spontaneous and SASE FEL radiation.

Concerning variation of the gain with the slit size, the increase in both energy spread and horizontal emittance as the slit opening is increased would only reduce the SASE gain. Thus a correction attempting to take into account the beam quality change associated with the slit scan will only serve to enhance our observed gain. Therefore, the signal enhancement beyond the (linear) spontaneous emission dependence on charge cannot be attributed to changes in the beam parameters.

Previous experiments (e.g., Ref. [9]) have seen signals from coherent spontaneous emission. We have strong evidence that our signal was not due to coherent spontaneous emission. One test used transition radiation from the pellicle near the wiggler. The transition radiation charge dependence, shown in Fig. 5, is measured using the same photodiode and interference filter as the wiggler emission, but with a collection angle large enough to include all the transition radiation. The charge was varied, as in the SASE studies, using the collimating slit. For transition radiation, the emission depends linearly on charge. The form factor governing the contribution from coherent transition radiation involves the same Fourier components of the electron beam distribution as does the form factor for coherent enhancement of spontaneous emission. Therefore, any coherent enhancement of the wiggler emission that scales with the square of the number of electrons should also be evident in the transition radiation measurement. The lack of this behavior demonstrates that the observed enhancement of spontaneous emission is not related to coherent enhancement. In addition, an electron beam structure on the micrometer scale is unlikely. This is supported by slice measurement of the wiggler emission shown in Fig. 3. Again using the time slice technique and transport-

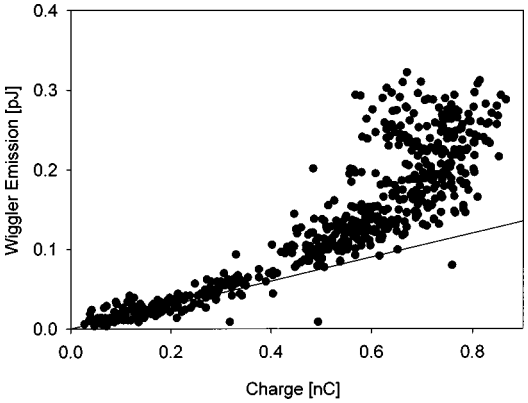

FIG. 6. Charge dependence of wiggler emission at 633 nm. The solid line is a fit to the spontaneous emission at low charge (optical emission before SASE sets in). Each point is an independent measurement pair of optical energy and beam charge. The scatter of the points results from the startup mechanism of SASE (see the text).

ing the portion of the electron bunch selected by the collimating slit through the beam line and wiggler, the optical emission of each slice is recorded. The emission is again limited to 1.0×10^{-3} rad and 25 nm around 1064 nm. The proportionality between wiggler emission and charge in each slice demonstrates that no individual slice is significantly enhanced and there is no evidence of any small scale structure in the bunch.

Additional preliminary evidence of SASE at visible wavelengths is observed by increasing the electron beam energy. Figure 6 shows the charge dependence of wiggler emission at 633 nm. Again, only on-axis emission was collected, and the bandwidth measured was 1 nm. This emission displays enhancement similar to that observed at 1064 nm, implying that any coherent enhancement at both wavelengths would require an even smaller structure to be present in the electron beam distribution.

The data in Figs. 4 and 6 also indicate another characteristic of SASE: the increase in fluctuation of the emission with increasing charge. This is expected because the total radiation emitted depends not only on the gain, which varies linearly with charge, but also on the spontaneous emission that is to be amplified. Fluctuation theory [17] predicts that for this pulse duration the intensity fluctuation should be 20% rms for 1064-nm emission, which agrees qualitatively with the measurement.

IV. THEORETICAL ANALYSIS AND COMPARISONS

The ratio of the SASE radiation spectrum over the spontaneous radiation spectrum is calculated approximately by two methods for comparison with the experiment. One is an analytical estimate, the other is an approximation by numerical simulation [17] using a three-dimensional version of the code TDA [18] based on a recently derived scaling relation between the output power and the number of simulation particles used in the code. These two methods agree with each other very well and provide an effective tool to analyze the experimental results.

A. Analytical estimate

The analytical estimate for start-up noise is based on a three-dimensional linear theory [19,20] for an electron beam with a step-function profile, zero energy spread, and zero angular spread. This idealized model for start-up noise is justified because the geometrical emittance is much smaller than the wavelength divided by 2π and the betatron wavelength (3 m) is much longer than two power gain lengths ($\approx$0.2 m), resulting in negligible betatron motion during the start-up process. The ratio of the SASE radiation spectral power in the guided mode, labeled by index n (excluding the spontaneous content) to the spontaneous radiation spectral power is given by [20]

$$\frac{\left(\frac{dP_{nm}}{d\omega}\right)_{\mathrm{SASE}}}{\left(\frac{dP}{d\omega}\right)_{\mathrm{spon}}}-1=\left(\frac{1}{9}\,e^{L_W/L_{G_n}}-1\right)\frac{2L_{G_n}}{L_W}\,\Gamma_n,$$

where P_{nn} and L_{G_n} are the power and gain length in the guided mode n, respectively. L_W is the length of the wiggler. The term Γ_n is the coupling factor of the radiation from the first two power gain lengths into the guided mode n and, along with L_{G_n}, is calculated in Ref. [20]. The term $(dP_{nn}/d\omega)_{\mathrm{SASE}}$ is the amplified spontaneous power in the guided mode, tending to the spontaneous power for no gain.

The label n used here actually represents an index that could be a set of several discrete indices. As explained in [20], the power is a sum over ''diagonal'' terms P_{nn} and ''cross'' terms P_{nl}. However, the cross terms P_{nl} are usually negligible. The measured ratio corresponds to a sum over all the modes and, since the gain is not high, includes the oscillating and decaying components as well.

Since the result is sensitive to the power gain length of the fundamental mode, it is calculated by the universal scaling gain function [21,22] for a waterbag model, which is close to the experiment. The difference between the waterbag model and the Gaussian model is negligible for our case, as long as we take the same rms emittance for both models. We assume the step-function distribution has the same rms beam size and peak current density as the waterbag model. The gain lengths for higher modes are estimated using the ratio of the scaled growth rate of these modes and the fundamental mode. This serves as a good approximation because the contribution from higher modes drops rapidly due to larger gain length and contributes little, as shown in the following.

B. Numerical simulation

In order to provide a numerical check of the SASE magnitude, the numerical simulation code TDA3D has been run for a wide range of emittances and currents. In a separate paper [23] we show how a single frequency code TDA3D can be used to simulate a phenomenon with finite bandwidth, such as the SASE process. Here we try to simulate the experiment at a fixed line by a scaling relation between power and the number of simulation particles.

In the linear regime, i.e., during the exponential growth before saturation, the average output power, which arises from shot noise (modeled by random loading), is inversely proportional to the number of simulation particles in an optical wavelength. Therefore, we estimate the time average output power $\langle P\rangle$ using the simulation output power $\langle P'\rangle$.

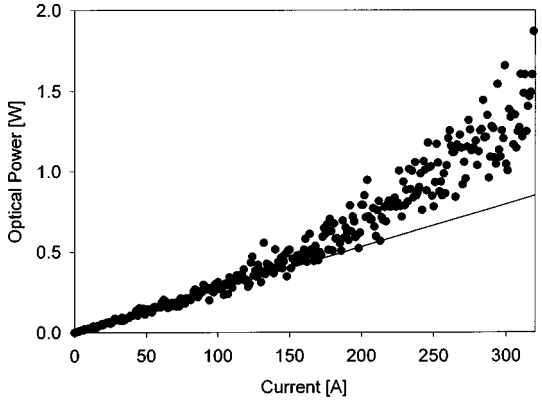

FIG. 7. Numerical simulation of wiggler emission as a function of beam current. This numerical simulation reproduces closely the measured wiggler emission in functional dependence, absolute value, and scatter of the individual ''shots'' (see the text).

$$\langle P\rangle = \frac{N'_\lambda}{N_\lambda}\langle P'\rangle,$$

where N_λ and N'_λ are the number of electrons and simulation particles within one optical wavelength, respectively. This conclusion is verified, by direct simulation, after averaging over many runs with different initial random electron distributions. We know, by comparing with the universal gain function [22], that 1200 simulation particles per cell are sufficient to predict the correct gain length for an amplifier. The azimuthal modes used in the calculation are from $m=-2$ to 2, i.e., five modes are used.

At the experimental conditions of $I=320$ and emittance of 0.7×10^{-6} m rad, the number of electrons within $\lambda_N = 1\ \mu$m is 6.7×10^6 and the output power given by TDA3D is 9×10^3 W. This is multiplied by $1200/6.7\times10^6$ to get the corrected simulation power of 1.5 W. As a further check, the theoretical spontaneous radiation power is obtained as follows. The brightness B_0 is

$$B_0 \equiv \left(\frac{\partial^2 P_{\rm spon}}{\frac{\partial\omega}{\omega}\,\partial\Omega}\right)\Bigg|_{\Theta=0,\omega=\omega_s} = \frac{e_0 Z_0 I\omega}{4\pi} N_W^2\gamma^2 \frac{K^2}{(1+K^2/2)^2}\mathcal{J}$$

$$= 5.72\times10^6 W,$$

where $Z_0=377\ \Omega$ is the vacuum impedance, e_0 is the electrons charge, K is the wiggler parameter, N_W is the number of wiggler periods, and $\mathcal{J}=\mathcal{J}_0[K^2/4/(1+K^2/2)] - \mathcal{J}_1[K^2/4/(1+K^2/2)]$ is the Bessel factor.

At $I=320$ A, the power for the wiggler's opening angle of $\Theta_W=\sqrt{2\lambda_s/L_W}$ and the bandwidth $1/N_W$ is estimated as $P_{\rm spont}\approx\pi\Theta_W^2 B_0(1/N_W)=1.1$ W. The extrapolated simulation spontaneous power is 0.75 W, in qualitative agreement with the spontaneous radiation theory value of 1.1 W. With more modes in the simulation the agreement can be made better.

Using this method and varying the current from 0 to 320 A, we plot the output power as a function of current in Fig. 7, where each point is an average over 30 runs. (30 is roughly the number of coherence lengths in a pulse length, see the discussion below.) The result shows that the power linearly increases with the current until approximately 100 A, corresponding to spontaneous radiation without gain, and then deviates from linear dependence at larger current. At 320 A the power is a factor 2 above the linear extrapolation from the spontaneous emission regime. Notice that the factor 2 also agrees with the analytical estimate 2.1 (see Sec. IV D).

Similar calculations have been done for various wiggler lengths, currents, and emittances. The results all approximately agree with the analytical estimates. When we increase the number of modes and correspondingly the number of simulation particles to achieve the correct growth rate, there is better agreement between spontaneous radiation theory and the simulation results. Using larger numbers of particles did not substantially change our results.

C. Intensity fluctuation

We also carried out a three-dimensional (3D) analytical analyses of the intensity fluctuation [24]. One particular result of our analysis is that in the 1D limit our 3D fluctuation formula is significantly simplified to

$$\frac{\sigma_W}{\langle W\rangle} = \frac{1}{\sqrt{l/l_c}},$$

where σ_W is the rms fluctuation of $\langle W\rangle$, the average output SASE energy per pulse, l is the length of a flat-top pulse, and l_c is a correlation length characterizing SASE coherence given by [17]

$$l_c = N_W\lambda_s\left(\frac{2\pi}{3}\frac{L_G}{L_W}\right)^{1/2},$$

where N_W is the number of wiggler periods, λ_s is the radiation wavelength, L_W is the wiggler length, and L_G is the power e-folding length. The relative fluctuation level is anticipated since we expect SASE to produce l/l_c pulselets, each with the same average spectral features and random phases.

The gain length, the electron beam pulse width, and the intensity fluctuations are simply related and can provide a useful consistency check for the theory and experiment. The comparison between the measured fluctuation level, the beam peak current, and the theoretical gain length will be done in the next section. Very similar spectral features are predicted for random backscatter of short laser pulses in a plasma [25].

D. Comparison with experiment

Based on the approximations discussed in Sec. IV A, the ratio for our case with a current of 320 A and an assumed normalized emittance of 0.7×10^{-6} m rad is calculated in the high gain limit as

$$\frac{\left(\frac{dP}{d\omega}\right)_{\text{SASE}}}{\left(\frac{dP}{d\omega}\right)_{\text{spon}}}-1=\left(\frac{1}{9}\,e^{0.53/0.11}-1\right)\frac{2\times 0.11}{0.53}\,(0.186)$$
$$+\left(\frac{1}{9}\,e^{0.53/0.16}-1\right)\frac{2\times 0.16}{0.53}\,(0.037\times 2)$$
$$+\cdots$$
$$\approx 0.98+0.08+\cdots\approx 1.1.$$

The wiggler is much shorter than the measured betatron wavelength (3 m). Therefore, we can approximate the beam size as constant even though there is no horizontal focusing and apply the formula given in [20]. For a longer wiggler, the treatment of Kim [26], which includes the angular spread of the beam would be appropriate. The gain length of 0.11 m is calculated using the formula given in [22], i.e., using the fact that the focusing is different from the natural focusing of the wiggler.

Each term is a contribution from one mode. The first term represents the fundamental mode with the azimuthal mode number $m=0$ and radial mode number $j=1$. The second term is for $m=1$ and $j=1$. The factor in front of the parentheses for each term is the gain for that mode. For higher modes these factors drop rapidly. To obtain the ratio of the SASE power including the spontaneous component to the extrapolated spontaneous power (no gain) 1 should be added, so that the expected ratio is ~ 2.1. The error due to neglect of higher-order modes is estimated at $\pm 10\%$.

This ratio is in agreement with the experimental result, as shown in Fig. 4. If we assume a larger emittance, the theory predicts a smaller ratio. The current of 320 A is as measured; however, the measured emittance is 50% larger than the measured slice emittance. The difference between the measured slice emittance and the emittance value that produces the best fit with the theory was discussed in Sec. III A. The differences in part due to the experimental electron distribution and the assumed theoretical distribution. The experimental distribution has non-Gaussian tails that increase the measured emittance value without a significant effect on the gain. As remarked earlier, the emittance is an incomplete descriptor of a complicated phase-space distribution. In addition, as can be seen from Table I, the measured emittance improves when a slice smaller than the whole bunch is measured. The local emittance of a slice smaller than what we can achieve with our resolution is expected to be smaller, in better agreement with the measured gain. Thus the uncertainties in the inputs to the model easily account for the differences between theory and experiment.

Another comparison can be made between the optical energy measurement and the simulation by observing the absolute values in Figs. 4 and 7. To do that we must correct for the bandwidth and angular opening in the measurement. The simulation is done for a bandwidth $1/N_W\sim 1/60$ and a full solid angle. For the small gain measured, the radiation bandwidth and opening angle should be almost the same as spontaneous radiation. Therefore, with the bandwidth of $1/N_W$, the radiation angle should be 1.9×10^{-3} rad. Now the measurement is made with a 25-nm filter, giving a bandwidth of 25 nm/1 μm$=\frac{1}{40}>1/N_W$, but the angular acceptance, set by a known aperture, is 1.0×10^{-3} rad. Thus the bandwidth is retained as $1/N_W$, but the solid angle is reduced by a factor $(\frac{1.0}{1.93})^2$. The simulated power total power at 320 A is a factor of 2 above spontaneous, which is extrapolated to 1.1 W at this current. There is some uncertainty in converting the simulated power to energy. As can be seen in Fig. 3, the current falls quickly as a function of time. Slices with a current less than 320 A will produce less SASE gain. If we divide the peak current by the measured pulse charge of 0.8 nC, we get an effective pulse width of 2.5 ps. Because of the gain dependence on the peak current, it would be wrong to use this number for the pulse width, and we estimate that 2 ps would be more appropriate. The pulse energy, with a pulse length of approximately 2 ps, is then $(\frac{1.0}{1.93})^2\times 2.2\times 2=1.1$ pJ. This is to be compared with the measured energy at the peak charge (corresponding to the peak current of 320 A) of 1.1 pJ. The agreement between the absolute values of the calculated and measured radiation energy is surprisingly good in view of the uncertainties discussed above.

Finally, we can compare the fluctuations in the shot-to-shot optical signal energy between the experiment and the theory outlined above. For our experiment, $\lambda\sim 1$ μm, $\lambda_W\sim 8.8$ mm, $I\sim 320$ A, $\varepsilon\sim 0.8\times 10^{-6}$ m rad, $E\sim 34$ MeV, and $L_g\sim 0.11$ m. The slippage is 60 μm and the coherence length is reduced to

$$60\ \ \mu\text{m}/\sqrt{\frac{3}{2\pi}}\times 4.9=40\ \ \mu\text{m}.$$

The pulse length is measured to be about 3.5 ps FWHM, i.e., about 1050 μm, hence the fluctuation $\sigma_W/\langle W\rangle$ is calculated to be about $\sqrt{40/1050}\approx 20\%$. This is consistent with the measured fluctuation of about 15%, considering that the pulse shape is actually not a step function and the calculated beam size is not really large enough to be near the one-dimensional limit. Nevertheless, the calculation serves as a rough estimate and a check that a description based on random noise is applicable.

V. CONCLUSIONS

In summary, we have extended the shortest-wavelength SASE measurements an order of magnitude over previous measurements using the MIT microwiggler, which provides high field quality at a period of 8.8 mm and a 34-MeV high-brightness electron beam at the Accelerator Test Facility. The charge dependence of wiggler emissions and optical transition radiation, longitudinal structure, and electron beam parameters required to theoretically predict SASE gain have been measured. We have considered alternative explanations other than SASE for the optical emission vs charge curves and eliminated these. The variation of beam properties such as emittance and energy spread as a function of charge, cannot mimic SASE in the measurements. The spontaneous optical emission along the electron bunch is proportional to charge of the measured ''slice.'' The optical detector linearity was tested in the range of measurements. An experimental measurement of transition radiation shows no evidence of coherent enhancement of spontaneous emission, and numeri-

cal and theoretical predictions are consistent with measured quantities for the spontaneous emission and SASE. We conclude that we have observed SASE in the infrared and visible regions. The favorable comparison of our measurements with theory based on particle noise startup suggests that the SASE model is valid.

ACKNOWLEDGMENTS

This work was performed under the auspices of the U.S. Department of Energy, under Contracts Nos. DE-AC02-76CH00016 and 02-91ER40669, and by Office of Naval Research Grant No. N00014-90-J-4130.

[1] M. Cornacchia, Proc. SPIE **2988**, 2 (1997).
[2] J. Rossbach, Nucl. Instrum. Methods Phys. Res. A **375**, 269 (1996).
[3] R. Prazeres, J. M. Ortega, F. Glotin, D. A. Jaroszynski, and O. Marcouille, Phys. Rev. Lett. **78**, 2124 (1997).
[4] A. L. Throop, W. M. Fawley, R. A. Jong, T. J. Orzechowski, D. Proznitz, E. T. Scharlemann, R. D. Stever, and G. A. Westenkow, Nucl. Instrum. Methods Phys. Res. A **272**, 15 (1988).
[5] D. Kirkpatrick *et al.*, Nucl. Instrum. Methods Phys. Res. A **285**, 43 (1989).
[6] S. Okuda, J. Ohkuma, N. Kimura, Y. Honda, T. Okada, S. Takamuku, T. Yamamoto, and K. Tsumori, Nucl. Instrum. Methods Phys. Res. A **331**, 76 (1993).
[7] D. Bocek, P. Kung, H.-C. Lihn, C. Settakorn, and H. Wiedemann, Nucl. Instrum. Methods Phys. Res. A **375**, 13 (1996).
[8] M. Hogan *et al.*, Phys. Rev. Lett. **80**, 289 (1998).
[9] K. W. Berryman, E. R. Crosson, K. N. Ricci, and T. I. Smith, Nucl. Instrum. Methods Phys. Res. A **375**, 526 (1996).
[10] D. A. Jaroszynski, R. J. Bakker, A. F. G. van der Meer, D. Oepts, and P. W. van Amersfoort, Phys. Rev. Lett. **72**, 3798 (1993).
[11] http://WWW.NSLS.BNL.GOV/AccTest/Menu.html.
[12] X. J. Wang, Nucl. Instrum. Methods Phys. Res. A (to be published).
[13] R. Stoner, and G. Bekefi, IEEE J. Quantum Electron. **QE-31**, 1158 (1995).
[14] P. Catravas, R. Stoner, and G. Bekefi, Nucl. Instrum. Methods Phys. Res. A **375**, 412 (1996).
[15] X. Qiu, K. Batchelor, I. Ben-Zvi, and X. J. Wang, Phys. Rev. Lett. **76**, 3723 (1996).
[16] P. Catravas, Ph.D. thesis, MIT, 1998 (unpublished).
[17] L. H. Yu and S. Krinsky, Nucl. Instrum. Methods Phys. Res. A (to be published).
[18] T. M. Tran and J. S. Wurtele, Comput. Phys. Commun. **54**, 263 (1989); B. Faatz, W. Fawley, P. Pierini, S. Reiche, G. Travish, D. Whittum, and J. Wurtele, Nucl. Instrum. Methods Phys. Res. A **393**, 277 (1997).
[19] L. H. Yu and S. Krinsky, Nucl. Instrum. Methods Phys. Res. A **285**, 119 (1989).
[20] S. Krinsky and L. H. Yu, Phys. Rev. A **35**, 8 (1987); **35**, 3406 (1987).
[21] L. H. Yu, C. M. Hung, D. Li, and S. Krinsky, Phys. Rev. E **51**, 813 (1995).
[22] L. H. Yu, S. Krinsky, and R. Gluckstern, Phys. Rev. Lett. **64**, 25 (1990); **64**, 3011 (1990).
[23] L. H. Yu (unpublished).
[24] L. H. Yu and S. Krinsky, Nucl. Instrum. Methods Phys. Res. A (to be published).
[25] G. Shvets, J. S. Wurtele, and B. Shliside, Phys. Plasmas **4**, 1892 (1997).
[26] K.-J. Kim, Nucl. Instrum. Methods Phys. Res. A **393**, 167 (1997).